Scaling of granular temperature in vibro-fluidized grains

Cite as: Phys. Fluids **28**, 043301 (2016); https://doi.org/10.1063/1.4944795
Submitted: 21 September 2015 . Accepted: 07 March 2016 . Published Online: 01 April 2016

Ashish Bhateja, Ishan Sharma, and Jayant K. Singh

PHYSICS OF FLUIDS **28**, 043301 (2016)

Scaling of granular temperature in vibro-fluidized grains

Ashish Bhateja,[1,2,a)] Ishan Sharma,[1,2,b)] and Jayant K. Singh[3,c)]
[1]*Mechanics and Applied Mathematics Group, Kanpur, India*
[2]*Department of Mechanical Engineering, Indian Institute of Technology Kanpur, Kanpur 208016, India*
[3]*Department of Chemical Engineering, Indian Institute of Technology Kanpur, Kanpur 208016, India*

(Received 21 September 2015; accepted 7 March 2016; published online 1 April 2016)

Granular temperature quantifies velocity fluctuations in fluidized granular materials. There is ongoing effort to understand granular temperature T in vibro-fluidized grains through the power law $T \propto V_p^{\alpha}$, where V_p is peak vibrational velocity. However, the present literature disagrees on the value of α. We utilize dimensional analysis and discrete element simulations to show that granular temperature, and therefore the exponent α, depends crucially on a non-dimensional number W representing the competition between vibrational and gravitational energies but is much less sensitive to other system parameters. Furthermore, change in the barycentric height Δh_{cm} of the vibrated grains, and their temperature T, typically behaves differently with V_p. Thus, Δh_{cm} cannot generally be used as a surrogate for T, as is often done at present. Our computations help explain the currently contradictory results on how granular temperature scales with peak vibrational velocity. Finally, we also briefly investigate the dependence of the temperature on system parameters, as well as its spatial variation. © *2016 AIP Publishing LLC.* [http://dx.doi.org/10.1063/1.4944795]

I. INTRODUCTION

Velocity fluctuations play a crucial role in understanding fluidized granular materials, such as rapidly flowing foodgrains or sand. These fluctuations are often quantified in terms of a *granular temperature* (T) that measures the fluctuational kinetic energy of the grains.[1,2] Granular temperature is, thus, analogous to temperature in the kinetic theory of gases[3] and forms the basis of all kinetic-theory based descriptions of flowing grains.[4,5]

Granular temperature in fluidized grains has been typically investigated in the context of vertically vibrated dissipative grains. The dependence of T on peak vibrational velocity V_p is often expressed through the power law

$$T = CV_p^{\alpha}, \tag{1}$$

where C is a constant, α is a scaling exponent, and $T = \int T(\mathbf{r})\, d\mathcal{V}(\mathbf{r})/\mathcal{V}$ is the volume-averaged granular temperature. Unfortunately, as the survey below shows, there is *no* consensus on the value of α. In this work, we demonstrate that including the acceleration due to gravity (g) helps clarify past contradictory results. Gravity enters the physics through the dimensionless number $W = V_p^2/dg$, where d is the grain diameter. The parameter W is the square of the ratio of the time scale induced by gravity ($\sqrt{d/g}$) to that due to the base motion (d/V_p); W, thus, quantifies the competition between the kinetic energy input through base vibrations ($\sim mA^2\omega^2$) and the gravitational potential energy ($\sim mdg$). It is easy to show that $\alpha = 2$ in the absence of gravity, notwithstanding system parameters, such as the number and shape of grains, their friction and restitution coefficients, vibration amplitude, and the presence or absence of sidewalls. However, when g is

a)Electronic mail: ashishbh@iitk.ac.in
b)Electronic mail: ishans@iitk.ac.in
c)Electronic mail: jayantks@iitk.ac.in

non-zero, α depends crucially on the range of W over which (1) is fit. Furthermore, while α may now be influenced by other parameters of the system, their effect is not found to be as strong as that of W.

Several previous investigations did *not* directly measure the temperature. Instead, they followed the change in the barycentric height Δh_{cm} of the vibrated grains and fitted the power law

$$\Delta h_{cm} = C_h V_p^{\alpha_h}, \tag{2}$$

where C_h is a constant and α_h is a scaling exponent. It was then assumed that $T \propto \Delta h_{cm}$, so that $\alpha = \alpha_h$. We will show that, in fact, T is *not* proportional to Δh_{cm}, except for large values of W.

Our findings have the following implications: (a) For large W, i.e., when external vibration dominates gravity, $\alpha \approx 2$ for *all* systems, (b) to study granular temperature T in intermediate regimes, we must match the range of W over which previous investigations are conducted, (c) in intermediate regimes, the change in the barycentric height Δh_{cm} cannot be utilised as a surrogate for T, and, finally, (d) if we wish to describe the behavior of T with V_p through power law (1), then a universal range of W needs to be identified, and we make one suggestion to this end in Sec. V.

Previous work shows no agreement on the scaling of granular temperature with peak vibrational velocity. The reasons underlying the disagreement are also *not* known. The analysis of Warr *et al.*[6] predicts that, in two dimensions, granular temperature scales with the square of V_p, i.e., $\alpha = 2$ in (1). This was confirmed by Kumaran[7] in both two and three dimensions. Huntley[8] proposed that $\alpha = 4/3$ in two dimensions, after heuristically extending the analysis of Warr *et al.* to dense systems. Meanwhile, the two-dimensional molecular dynamics simulations of Luding *et al.*[9] estimated that $\alpha = 1.5$. Two-dimensional experiments of Warr *et al.*[6] and Feitosa and Menon[10] found $\alpha = 1.41$ and 2, respectively. Yang and Candela[11] and Wildman *et al.*[12] conducted three-dimensional experiments and estimated α to be, respectively, 1 and 1.54. In binary mixtures, Wildman and Huntley[13] found that the temperatures of the small and big grains scaled as, respectively, $\alpha = 1.37$ and $\alpha = 1.41$, while Windows-Yule and Parker[14] found that the temperature of bi-disperse grains of the same size, but different materials, scaled with $\alpha = 1$. In all investigations, grains were vibrated from the bottom and did not interact with an upper boundary, if at all present. Some studies[9,11,14] did not measure T directly but inferred its scaling from that of Δh_{cm}, assuming that $T \propto \Delta h_{cm}$.

Finally, we distinguish the current work and its aim with previous computations[15,16] and analyses based on kinetic theory[17,18] or granular hydrodynamics.[19,20] The goal in these works was to study the spatial variations of fields such as temperature and volume fraction. No attempt was made to clarify why experiments did not agree on the scaling of the average temperature. In this paper, we address the latter issue.

II. DIMENSIONAL ANALYSIS

Here we investigate vertically vibrated, dissipative grains of mass m as shown in Fig. 1. Collisional dissipation is characterized by coefficients of restitution e_p and e_w for grain-grain and grain-wall interactions, respectively. The granular temperature T may be expressed through the functional dependence

$$T = f(g, V_p, A, d, m, N, e_p, e_w, \mu_p), \tag{3}$$

where A is the vibration amplitude and N is the number of layers in the granular assembly when it is static, e.g., $N = 4$ in Fig. 1. We ignore dependence on the Young's modulus, as elastic vibrations in a grain will play an insignificant role in the scaling of granular temperature. This is confirmed in Sec. V. The previous equation may be non-dimensionalized as

$$\overline{T} := \frac{T}{mV_p^2} = \overline{f}\left(\frac{V_p^2}{dg}, \frac{A}{d}, N, e_p, e_w, \mu_p\right). \tag{4}$$

The dimensionless number $W = V_p^2/dg$, which depends on gravity, arises naturally. The dependence of T on this number was, surprisingly, ignored in all previous investigations, even though, for vertically vibrated open systems, the restoring force on the grains is due only to gravity. Furthermore, in

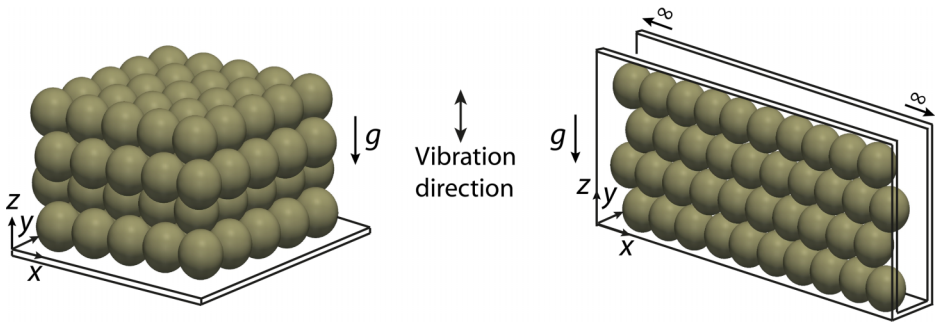

FIG. 1. Three- and two-dimensional assemblies of grains at rest on a rigid plane before being vibrated vertically along z.

all such systems, there is a natural competition between external vibrations, which fluidizes grains, and gravity, which causes grains to settle down. Comparing (4) and (1), it is clear that, when gravity is present, both C and α will depend on the range of W probed and on the parameters $A/d, N, e_p, e_w$, and μ_p. However, when g is absent, so is W, and, consequently, $\alpha = 2$, irrespective of the values of other parameters.

In subsequent development, we will investigate granular temperature through (4) by varying the dimensionless number W. Other parameters in (4) will be kept constant or changed systematically, as required. We will understand the effect of W on the granular temperature as capturing the importance of gravity's influence (gravitational potential energy) with respect to base vibrations. Indeed, the dimensionless number W only arises if gravity is present.

We note that non-dimensional numbers that include gravity have been employed previously, e.g., $A\omega^2/g$, where ω is the vibration frequency. However, their use was limited to providing a convenient representation of data. No effort was made to explain disagreement in the scalings of granular temperature on the basis of such numbers.

III. COMPUTATIONAL SETUP

With the elementary dimensional analysis in place, we turn to discrete element (DE) simulations, see Cundall and Strack.[21] Both two- and three-dimensional systems are studied, as shown in Fig. 1. Grains are spherical in shape, and their collisional interactions are modeled by means of a normal linear spring-dashpot model coupled with a tangential dashpot. Rough grains are described by including dry friction through a tangential Coulomb slider of friction coefficient μ_p. Appendix provides further details about our DE simulations.

A typical simulation begins with a collection of mono-disperse grains resting on a rigid base in the x-y plane. The base is vibrated vertically along z at $A\sin\omega t$. Finally, granular temperature is defined[1] as

$$T = \frac{m}{2d_f}\left(\langle u^2\rangle + \langle v^2\rangle + \langle w^2\rangle\right) =: \frac{\left(T_x + T_y + T_z\right)}{d_f}, \tag{5}$$

where u, v, and w are, respectively, the x, y, and z components of fluctuational velocity, d_f is the translational degrees of freedom of a grain, and $\langle\cdot\rangle$ denotes an ensemble average. All quantities are averaged over long times under steady-state conditions. Temperature may be anisotropic in the current granular system, so that we also define its x, y, and z components as above. Subsequently, we focus on the temperature component T_z, as appropriate for vertically vibrated grains. Thus, T_z replaces T in (1) and (4).

Experimental studies are necessarily conducted on confined grains. However, in simulations, we can prevent grains from getting influenced by sidewalls by considering a *canonical system*, obtained by imposing periodic boundary conditions in the horizontal x and y directions in three dimensions and along the x axis in two dimensions. The periodic cell is of size $5d \times 5d \times Nd$ in three dimensions and $10d \times Nd$ in two dimensions; we have verified that further increase in the

horizontal dimensions of the cell does not influence results. The frequency ω is varied from 300 rpm to 4000 rpm in increments of 100 rpm. For reasons detailed in Sec. IV, the vibration amplitude A is kept constant at one grain diameter. The spring-dashpot model, which describes grain collisions, is chosen to obtain coefficients of restitution $e_p = e_w = 0.9$, to match earlier experimental studies. Two cases are distinguished: (a) a *smooth system* in which the grains and the base have friction coefficient $\mu_p = 0$ and (b) a *rough system*, wherein the grains and the base have $\mu_p = 0.4$, corresponding to glass.

IV. RESULTS: EFFECT OF *W*

Figure 2 plots the variation of $\overline{T}_z = T_z/mV_p^2$ with the dimensionless number $W = V_p^2/dg$ for smooth and rough grains in both two and three dimensions. Here, W was varied by changing the frequency ω and fixing the amplitude ratio $A/d = 1$. This is done to isolate the effect of gravity that influences $\overline{T}$ in (4) through W. A change in the amplitude ratio will affect $\overline{T}$ in (4) directly and through W, as $W = V_p^2/dg = A^2\omega^2/dg$. This makes it impossible to distinguish between the contributions of W and A/d to variations in $\overline{T}$. Finally, note that altering ω or g in simulations is equivalent, as both only occur together in W, and not anywhere else in (4).

In all cases in Fig. 2, we observe that $\overline{T}_z$ initially increases with W, reaches a peak, and then decreases asymptotically to a constant value. We understand the behavior of $\overline{T}_z$ as follows. The temperature is a measure of the average fluctuational velocity of the grains that, in turn, depends on the collisional dynamics of the grains. In the absence of gravity, the collisional time scale is set by the rate $V_p = A\omega$ at which the rigid base is vibrated. There is *no* other time scale. This leads to $T_z \propto V_p^2$, i.e., $\overline{T}_z$ being a constant; the zero gravity case is further explored later in this section. Gravity will affect collisional dynamics *only* if the time scale d/V_p imposed by the vibrations is comparable to the time scale $\sqrt{d/g}$ over which gravity acts, i.e., when $(\sqrt{d/g})/(d/V_p) = W^{1/2} = O(1)$. This explains why $\overline{T}_z$ varies with W at low to moderate vibrations but asymptotes to a constant value at high W. We note that taking the limit $W \to \infty$ is equivalent to setting gravity to zero, where $\alpha = 2$.

The above arguments hold also for rough grains, as dissipation due to Coulomb friction is rate-independent. The key difference is that rough grains dissipate more energy and, so, move slower than smooth grains vibrated at the same rate. Therefore, at a given V_p, gravity influences collisional dynamics more in rough grains. Thus, $\overline{T}_z$ of rough grains in Fig. 2 decays to a constant at a rate slower than for smooth grains. The effect of system parameters e_p, μ_p, and N is discussed further in Sec. V.

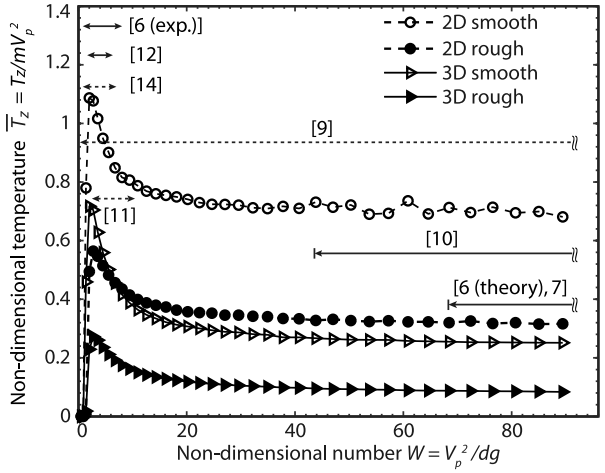

FIG. 2. Variation of $\overline{T}_z$ with W in the canonical systems defined in the text. We simulate 100 grains in three dimensions and 40 in two dimensions; this corresponds to an initial depth of four layers, i.e., $N = 4$. Also shown are ranges of W over which previous studies (identified by reference numbers) were conducted. Dashed ranges pertain to investigations that measured Δh_{cm} and not T_z.

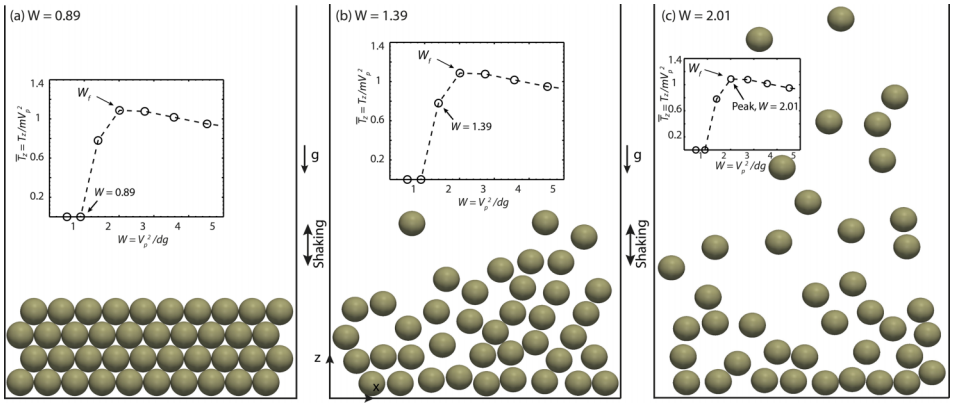

FIG. 3. Snapshots of a smooth two-dimensional system when vibrated at three frequencies that correspond to (a) $W < W_f$, (b) $W \lesssim W_f$, and (c) $W = W_f$, as shown in the insets.

The peak in the curves in Fig. 2 is related to the degree of fluidization of the granular assembly. We find that at W before the peak, V_p is low, and only the upper layers of the granular assembly are mobilized. As the vibration rate increases, so does W, and more layers get disturbed. At W beyond W_f — at which the peak in $\overline{T}_z$ occurs — all layers are observed to be agitated. We, thus, define the system to be *fluidized* when vibrated at $W > W_f$. The above argument is verified in Fig. 3 that shows snapshots of a vibrating two-dimensional system at three different W near W_f. In passing, we draw attention to the sudden increase in the granular temperature from zero at $W = 0.89$; see inset in Fig. 3. This is indicative of a solid to fluid transition that has also been seen[22] in horizontally shaken granular materials.

Figure 4 shows that the response of the non-dimensional horizontal and total temperatures, respectively, $\overline{T}_x$ and $\overline{T}$ is similar to that of $\overline{T}_z$. As expected, in a vertically vibrated system, T_x is lower than T_z. The total temperature is also lower, as it is the average of temperature in all directions.

The behavior of $\overline{T}_z$ in Fig. 2 appears generic for all vibrated systems where gravity plays a role, howsoever subtle. For example, Fig. 5 plots $\overline{T}_z$ in a *horizontally* vibrated channel. As shown in the inset, the grains are contained in an infinitely long smooth channel of width $43d$ and height $10d$, with base normal to gravity. We see that, when gravity is present, $\overline{T}_z$ first rises and then asymptotically decays to a constant, as in Fig. 2. Gravity plays a role because the grains can, and do, move normal to the channel's base, thereby regulating the dilatation of the grains. Thus, perhaps contrary to expectations, gravitational potential energy is important even in horizontally vibrated systems. In the absence of gravity, $\overline{T}_z$ is indeed a constant, as argued previously. We note that the second smaller peak in Fig. 5 is due to the grains striking the top of the channel at high W, which increases the agitation and thus the granular temperature.

Figure 6 plots the scaling exponent obtained in a three-dimensional, vertically vibrated system, after setting gravity to zero, but including an upper boundary to keep the grains from flying away. In this case, the non-dimensional number W is absent, and we change $\overline{T}_z$ by varying the amplitude ratio A/d and the initial number density n. In each case, the scaling exponent α is seen to be 2, as it must be on dimensional grounds discussed in Sec. II. The results of Fig. 6 are unaffected by the choice of N, e_p, and μ_p. These results, therefore, reinforce the suggestion that the presence of gravity, as captured by W, is the fundamental reason that α varies. This is confirmed in Sec. V, where we show that α depends only weakly on system parameters when $g \neq 0$.

Figure 2 also identifies the range of W over which previous studies were conducted. From the figure, it is clear that, in vertically vibrated grains, the exponent α in (1) will depend on the range of W over which power law (1) is fit. In fact, the behavior of $\overline{T}_z$ in Fig. 2 suggests that, except at high W, seeking a power-law description of kind (1) may be an oversimplification, and we explore this issue at the end of this section. For the moment, we continue to work with the hypothesis that a power-law scaling may be obtained. This is done to make contact with past and ongoing research

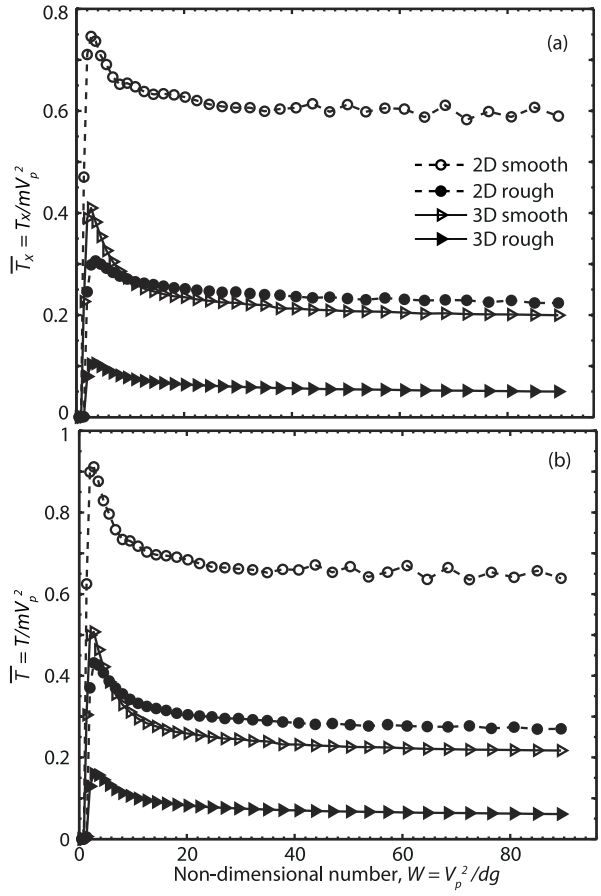

FIG. 4. Variation of non-dimensional temperatures $\overline{T}_x$ and $\overline{T}$ with W in the canonical systems defined in the text.

that assume such power laws and, further, to emphasize how properly accounting for gravitational potential energy, through the non-dimensional number W, helps reconcile previous disparate results.

A quadratic scaling, i.e., $T_z \propto V_p^2$, will only hold when attention is restricted to high enough W, as in kinetic theory based analyses,[6,7] which tacitly assume that external force fields, like gravity,

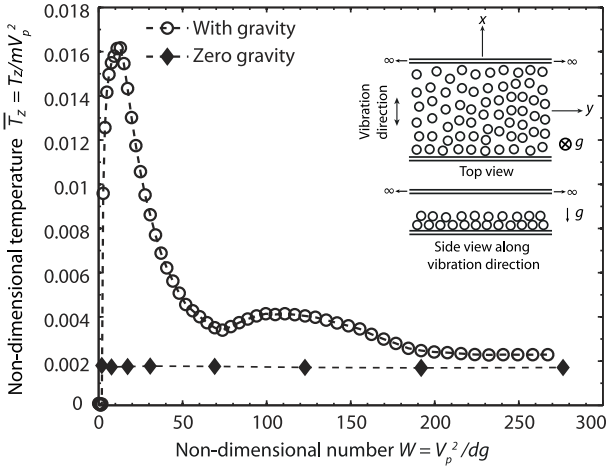

FIG. 5. Variation of $\overline{T}_z$ with W in *horizontally* vibrated smooth grains, with and without gravity. Periodic boundary conditions are imposed along the y-axis, and the channel is vibrated along the x-axis. We simulate 3000 grains, with $N = 2$, 40 rpm $\leqslant \omega \leqslant$ 900 rpm, $A = 10d$, and $e_p = e_w = 0.3$.

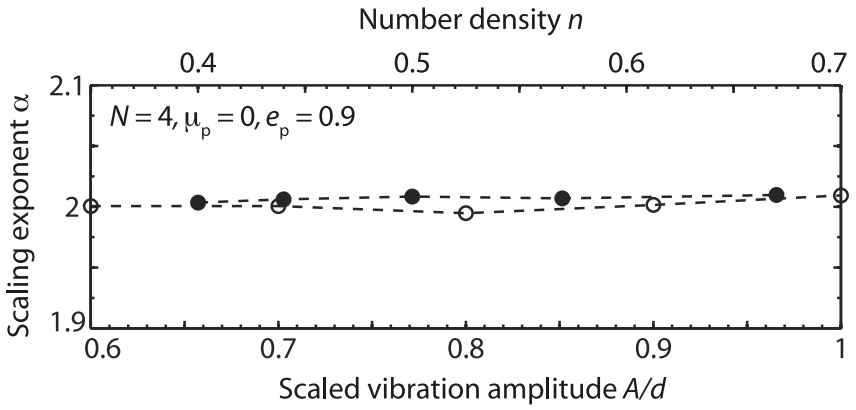

FIG. 6. The scaling exponent α obtained when grains are vibrated vertically with $g = 0$. The rigid upper boundary is $10d$ away from the base. Several amplitudes A (open circle) and initial number densities n (filled circle) are investigated.

do not affect collisional dynamics. Huntley[8] claimed that α depends crucially on the number density n via the mean free path l. Assuming that the average coordination number s is six in dense two-dimensional systems, Huntley found that $l \sim 1/\sqrt{n}$. This is in contrast to the estimate of $1/n$ for gases at equilibrium. As suggested by Fig. 6, and shown by experiments discussed at the end of Sec. V, W, and *not* n, is fundamentally responsible for variations in α. Furthermore, we find that largest value of the average volume fraction, seen at the peak in Fig. 2 when $W = W_f$, is about 0.2. This is much smaller than ~0.7, which is the volume fraction when $s \approx 6$. This is expected as s is six only in crystallized systems.[23] Thus, Huntley's explanation may not be entirely satisfactory.

Next, for each previous experimental study, we employ (1) along with the curves in Fig. 2, over the associated range of W, to compute the exponent α. We emphasize that the limited ranges of W over which $\overline{T}_z$ is fit are dictated by experiments and are not our choices. The simulations of Luding *et al.*[9] are atypical and are considered separately. For comparison with experiments, we consider the two- or three-dimensional rough systems, as appropriate. The results are tabulated in Table I. We see that our computed scalings are close to what have been observed by experiments that measure temperature directly. The small deviations from these experiments are primarily because of two reasons. First, experiments, as opposed to our canonical system, are conducted in boxes where the presence of sidewalls affects α. This effect is complex, as it depends on the frictional and damping characteristic of the walls and their separation. Second, we model normal collisions through a linear spring-dashpot model, which leads to the restitution coefficient e_p being independent of collisional velocity.[24] Experiments[25,26] show that e_p reduces as the collisional velocity increases. In fact, in adhesive grains, e_p may reduce even for low-speed collisions.[27,28] The overall effect is to increase dissipation, especially at higher agitation levels. This, as for rough systems in Fig. 2, will slow the rate at which $\overline{T}_z$ decays to a constant, thereby reducing α. McNamara and Falcon[29] confirm that α indeed lowers when e_p is velocity-dependent, cf. Sec. V.

TABLE I. Comparison of the scaling exponent α reported in previous studies with those found from Fig. 2, in the manner discussed in the text. References in bold measured temperature scaling directly, while the others inferred it from Δh_{cm}.

Reference	α (reference)	α
Warr *et al.*[6]	**1.41 ± 0.03**	**1.49**
Wildman *et al.*[12]	**1.54 ± 0.37**	**1.43**
Feitosa and Menon[10]	**2**	**1.92**
Yang and Candela[11]	1 ± 0.2	1.12
Windows-Yule and Parker[14]	0.92 ± 0.1	1.29

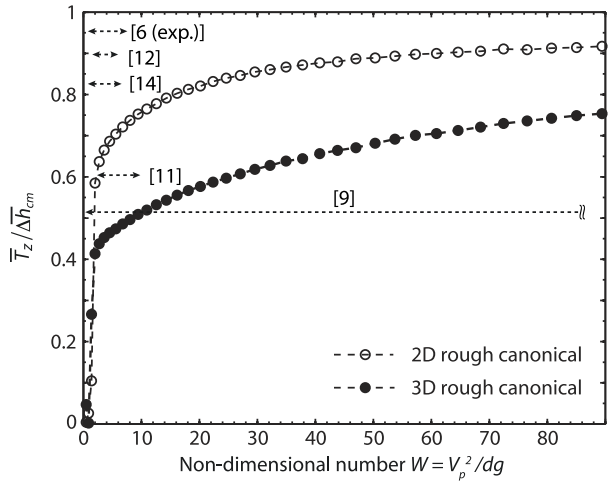

FIG. 7. Variation of the ratio $\overline{T}_z/\Delta\overline{h}_{cm}$ with W in two- and three-dimensional rough canonical systems. The simulation parameters are same as in Fig. 2. Also shown are ranges of W over which studies listed in Table II were conducted.

Our results differ from those reported by references in the bottom two rows of Table I, because those studies inferred the scaling of temperature from that of the change in the barycentric height Δh_{cm}. Even earlier, experiments[6,12] have observed different scalings α and α_h for, respectively, T_z and Δh_{cm}. Figure 7 shows that the ratio $\overline{T}_z/\Delta\overline{h}_{cm}$, where $\Delta\overline{h}_{cm} = \Delta h_{cm}/\left(V_p^2/g\right)$, is a constant only at high W. However, over intermediate ranges of W, where most experiments are conducted, the behaviors of $\overline{T}_z$ and $\Delta\overline{h}_{cm}$ are not the same, so that α and α_h differ. This is confirmed in Table II, which compares experimental observations of α_h with exponents that we obtain, after fitting (2) with our simulation data over the W-range that the experiments probed. We now find a good match with experiments. Thus, α and α_h are typically different, and we should *not* expect temperature to behave in the manner in which the height of the center-of-mass shifts. Indeed, the barycentric height was employed as a proxy for the temperature only after assuming that the number density n is given by the Boltzmann distribution, $n \propto e^{-mgz/k_BT}$, where k_B is the Boltzmann constant. This assumes an isothermal granular system. However, we have seen above that the temperature does not scale quadratically, so that the granular system being investigated is *not* isothermal; the results of Sec. VI support this conclusion further. Thus, there is little reason to expect that the temperature and the barycentric heights will scale in the same manner. This has important implications on how barycentric shifts in vibro-fluidized grains should be interpreted.

We turn, finally, to the simulations of Luding *et al.*[9] They followed Δh_{cm} for $0 \leqslant W \leqslant 750$ and computed $\alpha_h = 1.5 \pm 0.01$. But, as Table II shows, *no* experiments have observed this scaling, even though *all* experiments were conducted over ranges covered by simulations.[9] This may be because of specific details of their computation that are inaccessible to us.

We end this section by attempting to fit the curves of Fig. 2 through both an algebraic and an exponential dependence of $\overline{T}_z$ on W, respectively, $\overline{T}_z = a\left(1 + cW^{-b}\right)$ and $\overline{T}_z = a\left(1 + ce^{-bW}\right)$, where a, b, and c are fitting constants. The results are shown in Fig. 8 on both linear and log scales, and the fitting constants and the correlation coefficients are summarized in Table III. We fit the

TABLE II. Comparison of the scaling exponent α_h reported in previous studies with those found from our simulations.

Reference	α_h (reference)	α_h
Warr *et al.*[6]	1.3 ± 0.04	1.41
Wildman *et al.*[12]	1.24 ± 0.15	1.19
Yang and Candela[11]	1 ± 0.2	0.88
Windows-Yule and Parker[14]	0.92 ± 0.1	1.06

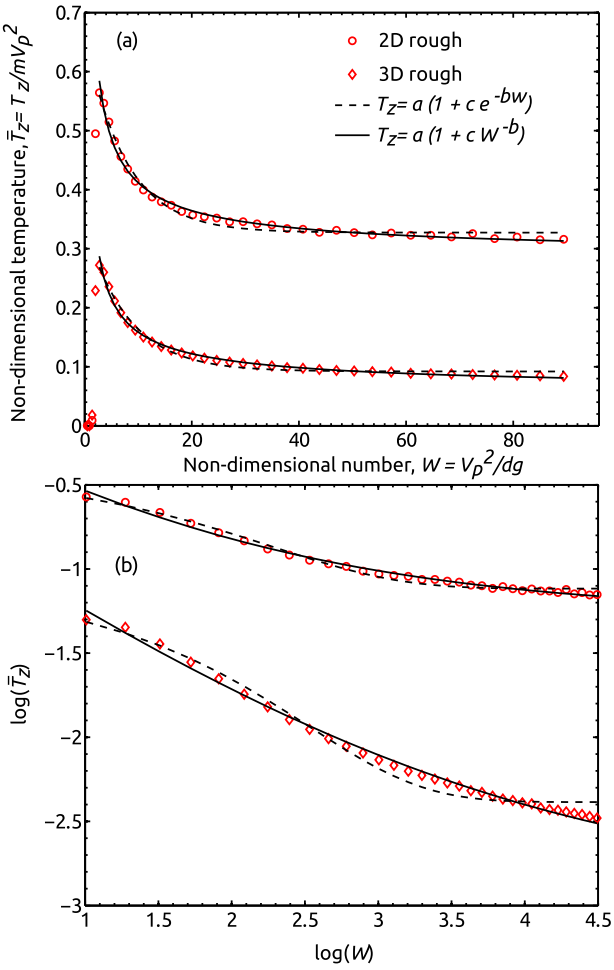

FIG. 8. Algebraic and exponential fits of $\overline{T}_z$ and W in rough two- and three-dimensional systems.

temperature behavior only after fluidization, i.e., after the peak in the curves of Fig. 2. Even though the correlation coefficients for all fits are comparable, it is clear from Fig. 8(b) that an algebraic dependence is better in both two- and three-dimensional systems, while the exponential fit reveals systematic errors,

$$T_z = c_1 V_p^2 + c_2 V_p^{\alpha}. \tag{6}$$

This, in turn, suggests that the (volume-averaged) temperature T_z is best related to the peak vibrational velocity as a sum of two power laws: with constants c_1 and c_2, and $0 < \alpha < 2$; the first term captures behavior at high V_p, while the other governs the temperature response at low to moderate vibration rates.

TABLE III. Fitting parameters employed in Fig. 8.

System	Fit	a	b	c	Correlation coefficients
2D rough	Algebraic	0.282	0.656	2.07	0.9957
2D rough	Exponential	0.327	0.131	1.022	0.9941
3D rough	Algebraic	0.054	0.622	7.98	0.9964
3D rough	Exponential	0.092	0.124	2.695	0.9943

V. RESULTS: EFFECT OF SYSTEM PARAMETERS

In this section, we investigate the dependence of the granular temperature and the scaling exponent α on various system parameters, which includes the grain stiffness as characterized by the normal spring stiffness k_n (see the Appendix), e_p, μ_p, N, and the amplitude ratio A/d.

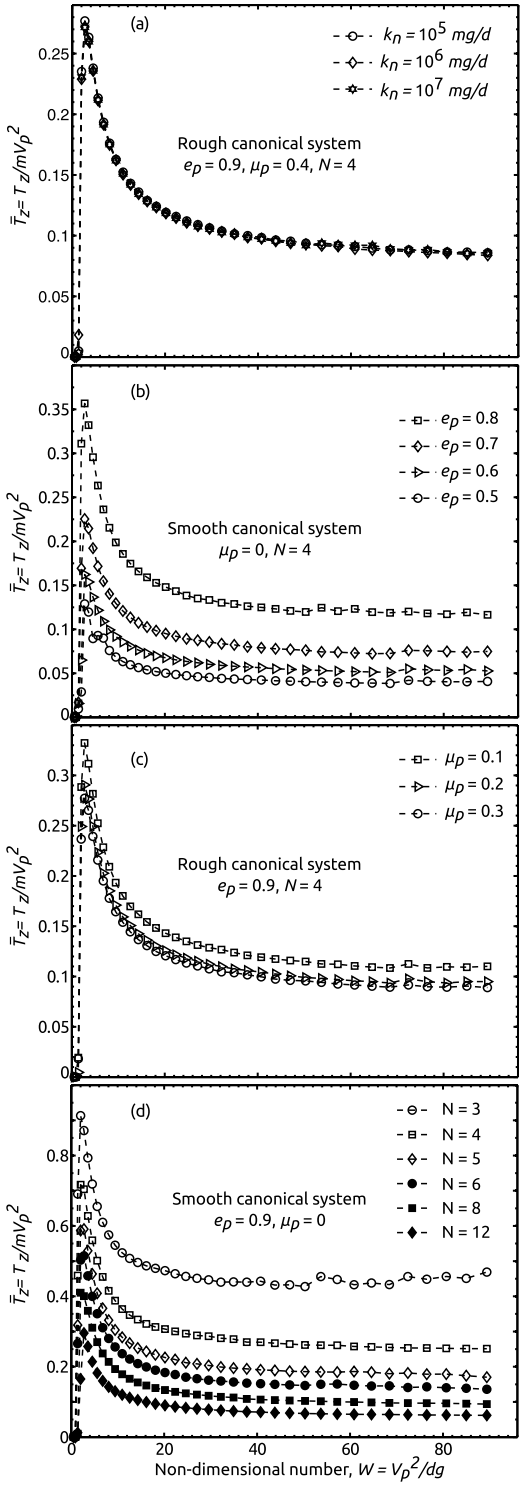

FIG. 9. Variation of the non-dimensional temperature $\overline{T}_z$ with W at different (a) k_n, (b) e_p, (c) μ_p, and (d) N.

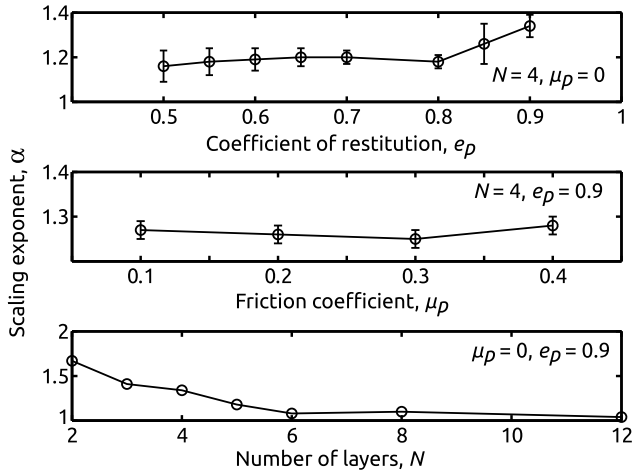

FIG. 10. Dependence of α on e_p, μ_p, and N.

To study the effect of k_n, e_p, μ_p, and N, we repeat the simulations of Sec. IV, while varying any one of these parameters. Throughout, the amplitude ratio A/d is kept fixed at 1, for reasons already mentioned in Sec. IV. The results are shown in Fig. 9. Figure 9(a) confirms our claim in Sec. II that grain stiffness does not affect the granular temperature. At the same time, Figs. 9(b)–9(d) show that, for each choice of e_p, μ_p, and N, the non-dimensional temperature $\overline{T}_z$ behaves as in Fig. 2, except that the curves are stretched or squeezed, depending on whether the overall dissipation increases or decreases. This holds even for deep ($N \geqslant 6$) beds in Fig. 9(d). We also observe that, amongst e_p, μ_p, and N, the granular temperature is most impacted by changes in the number of initial layers N and least by the friction coefficient μ_p.

Next, for each simulation of the kind shown in Figs. 9(b)–9(d), we compute α by fitting (1) over a range of W that extends from W_f, where the system fluidizes completely, to W_2, beyond which $\overline{T}_z$ is nearly constant. The range $[W_f, W_2]$ is one candidate for a universal range over which to explore the power-law dependence of T_z in vibro-fluidized systems.

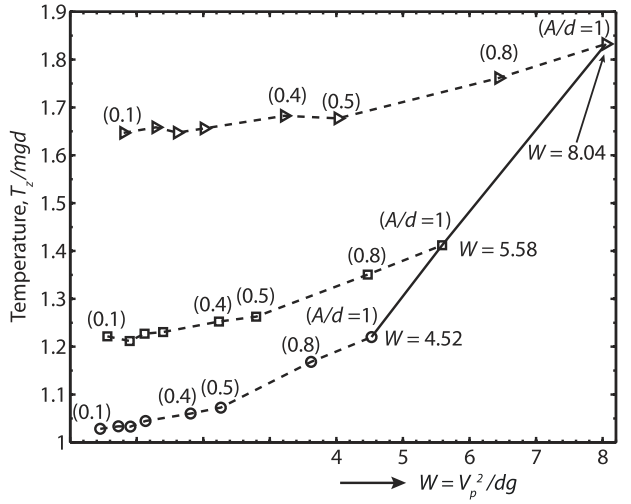

FIG. 11. Dashed lines show variation of the scaled temperature T_z/mgd with amplitude ratio A/d at three values of W. Each dashed line originates from a point with specified W, either 4.52, 5.58, or 8.04. Along a dashed line, A/d decreases from 1 to 0.1, as indicated in parenthesis, while W is kept constant by changing ω proportionately. Along the solid line, W is increased from 4.52 to 8.04 by incrementing ω, but keeping $A/d = 1$. We consider a rough two-dimensional canonical system. The abscissa relates to the solid line.

Figure 10 shows the effect of changing e_p, μ_p, and N on α. When grains are more elastic, i.e., e_p is more, the grains move faster at a given V_p, and changes in gravitational potential energy are less significant. Thus, $\overline{T}_z$ in Fig. 9(b) becomes constant more rapidly, i.e., W_2 is lowered; the more rapid decay of $\overline{T}_z$ at higher e_p is clear from Fig. 9(b). This leads to α increasing with e_p, albeit gently. On the other hand, when N is large, there is a bigger mass of grains and a corresponding greater importance of gravitational potential energy. Indeed, Fig. 9(d) shows that $\overline{T}_z$ becomes constant at a slower rate at higher N. Thus, W_2 is elevated, and, so, α decreases. It is interesting to note that α becomes nearly constant at about 1 for deep beds, i.e., for beds with $N \geqslant 6$. Finally, we observe that changing μ_p affects α only marginally, but in a manner similar to e_p, for the same reasons. Our results for e_p and N are consistent with previous findings.[29]

Past experiments varied the initial number of layers N. We now show that the effect of gravity on the scaling exponent α, as captured by W, is much more pronounced than that of N, for the values of N considered. Yang and Candela[11] and Windows-Yule and Parker[14] did experiments with deep beds, respectively, $N \leqslant 7$ and $3 \leqslant N \leqslant 10$. Noting from Fig. 10 the minimal effect of N when

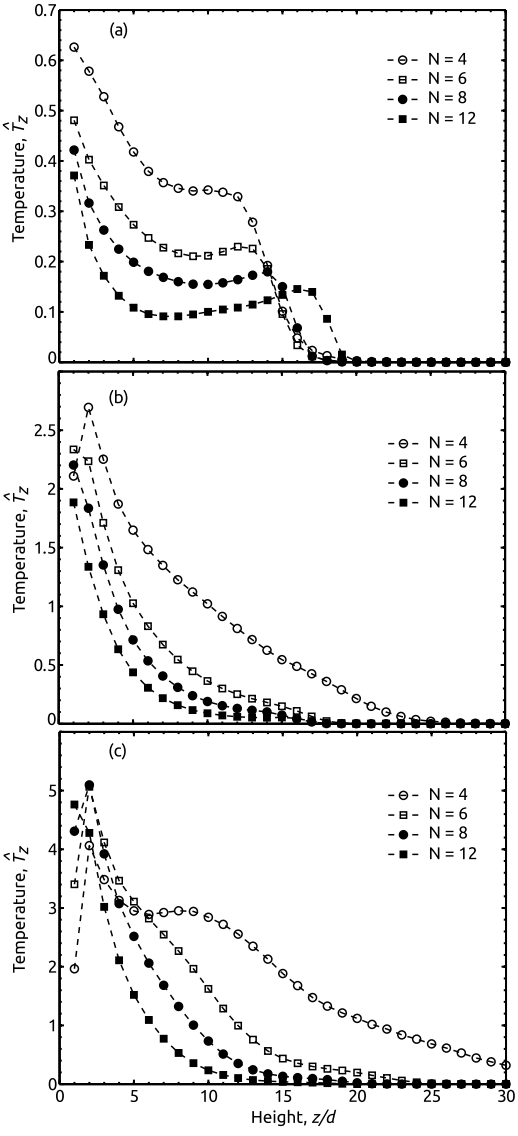

FIG. 12. Variation in local temperature $\hat{T}_z$ with z for several N at (a) $W = 5.58$, (b) $W = 22.35$, and (c) $W = 50.3$ in a three-dimensional, smooth canonical system with $e_p = 0.9$.

$N \geqslant 6$, we repeat our simulations with $N = 6$ over the W range that these researchers probed. We find marginal changes in the scaling exponent α_h from what is reported for $N = 4$ in Table II. In the case of Yang and Candela, α_h changes to 0.75, while for Windows-Yule and Parker, we find $\alpha_h = 0.92$. The former is within experimental error, while the latter matches experiments.

Another demonstration of the greater importance of W compared to N is as follows. Experiments of Warr *et al.*[6] were done at W between 0.5 and 9 for $N = 1, 2$, and 3. For $N = 3$, α was 1.41, and *no* appreciable difference was seen at other N. Thus, even though N varied, α remained the same because of the fixed range of W. At the same time, Feitosa and Menon[10] covered W between 44 and 135, took $N = 4$, and observed $\alpha = 2$. Both Warr *et al.* and Feitosa and Menon conducted experiments with grains of similar properties. Figure 10 shows that changing N from 3 to 4 barely affects α. Therefore, the discrepancy in the observed scalings must be because the two experiments were conducted over distinct ranges of W. This, recall, corresponds to different relative importance of the gravitational potential energy in comparison to the vibrational kinetic energy supplied by the base.

We have so far shown that, in (4), the effect of W on $\overline{T}$ is far more significant than that of N, e_p, and μ_p when the amplitude ratio A/d is set equal to 1. This implies that, if A/d is held constant — as in all simulations so far — gravitational potential energy, through W, regulates $\overline{T}$ and so also the scaling exponent α. However, most experiments control the amplitude ratio rather than the frequency. When the amplitude is varied, it also changes $W = V_p^2/dg$, as $V_p = A\omega$. This makes it impossible to distinguish the impact of W on granular temperature from that of A/d, cf. (4). We note that alteration in W due to variation in A/d indicates how kinetic energy input by the base ($\sim mA^2\omega^2$) compares with gravitational potential energy ($\sim mdg$). Thus, the part of the response

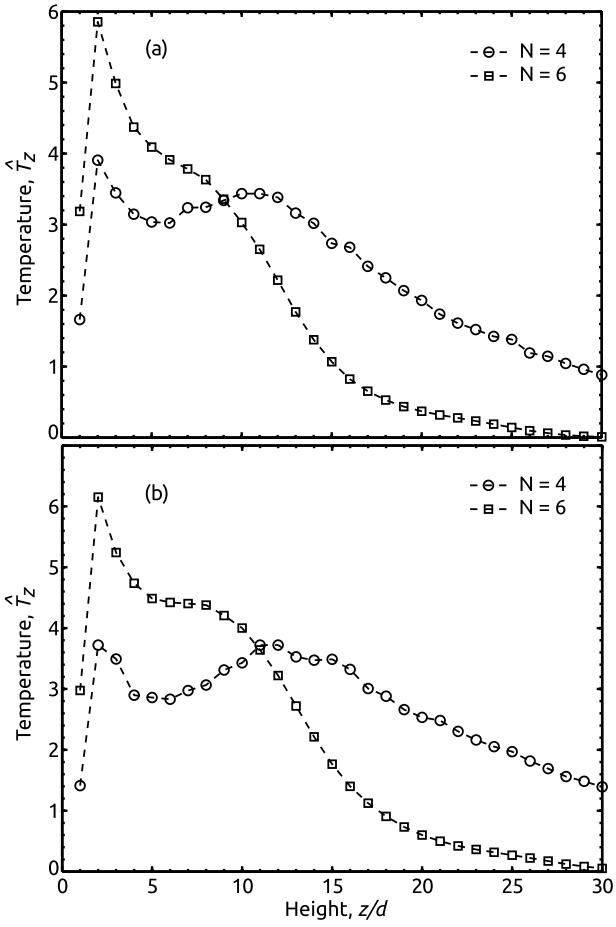

FIG. 13. Continued from Fig. 12. Variation in $\hat{T}_z$ with z for a shallow and a deep bed at (a) $W = 68.46$ and (b) $W = 85.01$.

of $\overline{T}$ that is driven by changes in W — introduced by variations in A/d — reflects the influence of gravity on $\overline{T}$. We now wish to show that the observed scalings in experiments, which controlled A/d, were primarily due to corresponding changes in W modulating $\overline{T}$. To this end, we demonstrate that granular temperature is not affected much when we vary A/d, but keep W fixed.

Figure 11 compares how the granular temperature T_z — now scaled by mgd — changes when we vary the amplitude ratio A/d but keep W fixed at three different values (dashed lines), to the case when we change W keeping $A/d = 1$ (solid line). We investigate a range of W corresponding to the experiments of Warr *et al.*[6] The solid line in Fig. 11 shows that when we span this W-range retaining $A/d = 1$, the temperature increases by nearly 50%. On the other hand, when we decrease A/d from 1 to 0.1 along any dashed line in Fig. 11, while W is kept fixed at the value from which the dashed line begins, we find that the temperature reduces by only 15% on average. Moreover, when we restrict ourselves to the range of amplitude ratios probed by Warr *et al.*, i.e., A/d between 0.1 and 0.5, the average change in temperature is a mere 3%. These simulations confirm that the effect of W on granular temperature, and hence its scaling, is far more significant than that of the amplitude ratio A/d.

VI. RESULTS: SPATIAL VARIATION

As mentioned in the Introduction, a vertically vibrated system is not homogeneous. In this final section, we briefly investigate how temperature varies spatially in our canonical systems. In these systems, sidewalls are absent, and spatial variation indicates change with vertical height z. To this end, we compute the *local* temperature $\hat{T}_z(z)$ at a vertical station z by averaging the temperature T_z

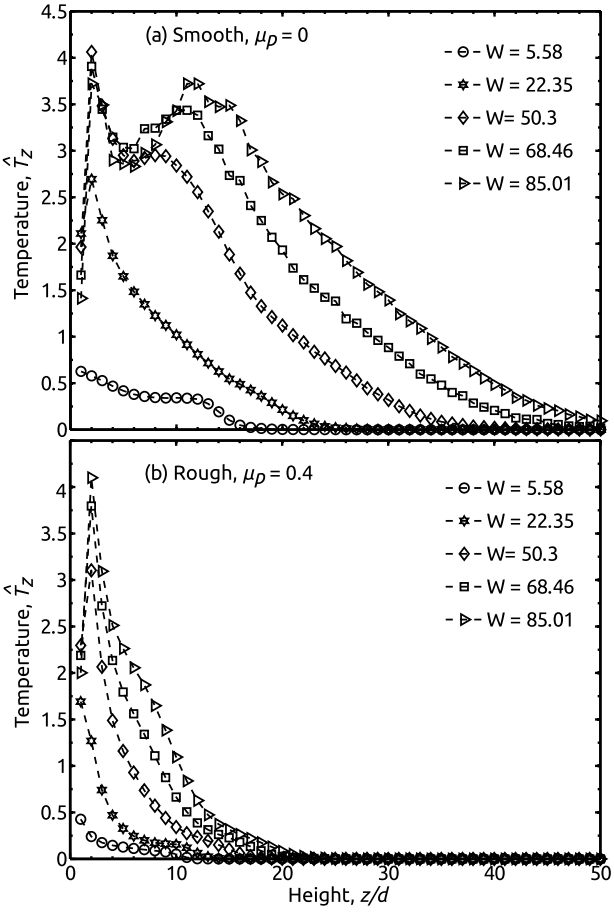

FIG. 14. Variation of $\hat{T}_z$ in three-dimensional smooth and rough systems with $e_p = 0.9$. We use 100 grains and $N = 4$.

in a horizontally aligned box of depth one particle diameter that is centered at z. Finally, we will primarily focus on three-dimensional systems, as two-dimensional systems display qualitatively similar response.

We had earlier, in Fig. 9(d), contrasted the behavior of the (volume averaged) temperature T_z with the parameter W for various initial numbers of layers N. We had observed that the temperature curves were similar for both shallow and deep beds. Typically, a bed is "shallow" if the initial number of layers $N < 6$ and "deep" if $N \geqslant 6$, see, e.g., Wassgren *et al.*[30] This similarity is reinforced when we consider the spatial variation of temperature for several N at different values of W; these results are shown in Figs. 12 and 13.

In Fig. 12(a), the temperature $\hat{T}_z(z)$ is seen to initially decrease with height from the base, as expected. However, interestingly, all beds display a low secondary peak in their temperature profiles immediately before the temperature rapidly vanishes. As W increases to 22.35 in Fig. 12(b), this secondary peak subsides. Additionally, the hottest region shifts from being next to the vibrating base, to 7-10 grain diameters above. This feature is initially observed for shallow beds, but, at higher W also for deep beds, see Fig. 12(c). At $W = 50.3$ in Fig. 12(c), we find that the low secondary peak returns in the shallow bed ($N = 4$). Again, as W increases, deep beds too demonstrate this feature, see Fig. 13. We also see that the secondary temperature peak increasingly becomes more prominent at high W. In fact, at $W = 85.01$ in Fig. 13(b), the secondary temperature peak is comparable to the primary one next to the base for the shallow bed with $N = 4$.

Simulations with deep beds are computationally very expensive. However, noting the qualitative similarities between the responses of both the average and the spatial temperatures in shallow and deep beds, further investigations will be primarily for beds with $N = 4$. The understanding is that the behavior observed for $N = 4$ will also be shown by deeper beds, albeit at higher W.

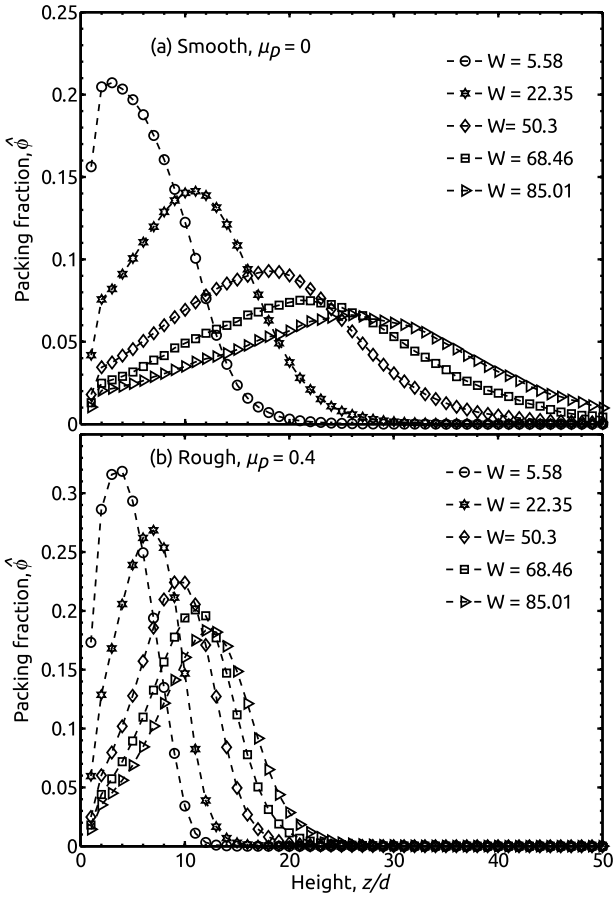

FIG. 15. Variation of $\hat{\phi}$. See also caption of Fig. 14.

We have confirmed the validity of this hypothesis by comparing with results from simulations for three-dimensional, smooth, deep beds. This is not shown for brevity.

We now compare the vertical variation of the local temperature $\hat{T}_z(z)$ and the packing fraction $\hat{\phi}(z)$ at several values of the parameter W for three-dimensional systems; these are shown in Figs. 14 and 15, respectively. As anticipated, $\hat{T}_z(z)$ in Fig. 14 increases with W. We see that in most cases, perhaps counterintuitively, the "hottest" region is not next to the vibrating base but at a distance slightly away, cf. Figs. 12 and 13. This feature is lost at low W and with higher friction, perhaps due to reduced mobility of the grains. We also note that at all W, the temperature decays to zero with height, with non-zero $\hat{T}_z$ persisting for greater z at higher W as, then, grains reach higher elevations, cf. Fig. 15. Finally, we observe the presence of a secondary peak in Fig. 14(a), which becomes increasingly more prominent at higher W but vanishes when friction increases in Fig. 14(b), perhaps, due to reduction in granular mobility. These results are in agreement with the computations of Lan and Rosato.[15] However, we only have partial match with the hydrodynamic analysis of Brey *et al.*[20] which, in contrast to Fig. 14(a), predicted a monotonic decay in the temperature after an initial maximum.

Similarly, but more prominently, the packing fraction too peaks a few grain diameters away from the vibrating base, before falling away to zero as we move away from the base, see Fig. 15. This maximum does not occur at the same location as the primary peak in $\hat{T}_z$ in Fig. 14. No secondary peak is seen. The packing fraction profile may be understood heuristically on the basis of opposing effects of the vibrating base and downward gravity: while collisions with the base drive grains upwards, gravity causes them to fall down, and these two "streams" of grains coalesce some distance away from the base. Figure 15 also shows that the packing fraction in rough systems peaks earlier, and their maximum packing fraction is also higher. The earlier peaking again reflects the fact that when dissipation is present, grains energized by collisions with the base slow down faster, leading to clustering closer to the wall.

At the same time, dissipative grains will cluster more, resulting in higher packing fractions. For a given system, a similar argument explains the earlier peaking of the volume fraction at lower W — when W is low, gravity's effect is greater, and the grains energized by the base meet the ones falling under gravity closer to the base.

Finally, in Fig. 16, we plot the scaled local temperature $\hat{T}_z/mV_p^2$ at various vertical stations as functions of W in two- and three-dimensional, smooth and rough systems. In two-dimensional

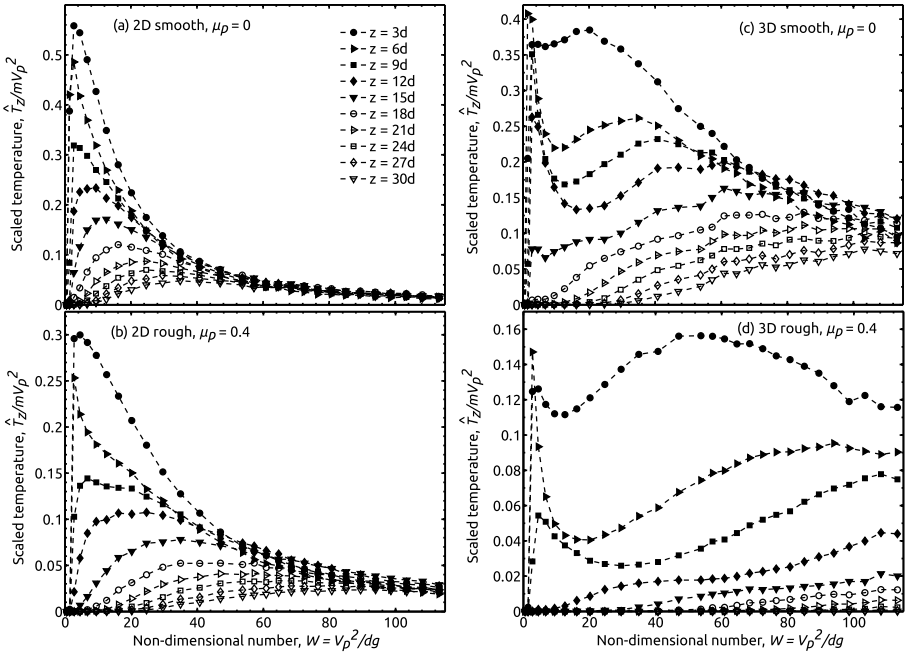

FIG. 16. Variation in scaled local temperature $\hat{T}_z$ with W at different vertical locations z in two- and three-dimensional, smooth and rough systems with $e_p = 0.9$ and 100 grains, so that $N = 4$. The legend for different z-curves is provided in (a).

systems, we find that $\hat{T}_z$ becomes a constant at higher values of W, see Figs. 16(a) and 16(b). Thus, $\hat{T}_z$ also scales as V_p^2 at higher W, and this is consistent with the response of the scaled volume-averaged temperature $\overline{T}_z$ in Fig. 2. In three dimensions, Figs. 16(c) and 16(d) show that the decay of $\hat{T}_z/mV_p^2$ to a constant value is slower. In each case, surprisingly, the scaled volume-averaged temperature $\overline{T}_z$ asymptotes to a constant faster in Fig. 2 than do the local temperatures $\hat{T}_z/mV_p^2$ in Fig. 16. This may be understood from Fig. 16 where, at low z, the temperature is greater than average and decreases with increasing W. At the same time, high-z regions are colder than average but become hotter as W grows. The local temperatures at low and high z tend to balance out, and the volume average becomes a constant before $\hat{T}_z/mV_P^2$.

VII. CONCLUSION

In this work, we have demonstrated that granular temperature T of vibro-fluidized grains depends crucially on gravity g through the non-dimensional number $W = V_p^2/dg$, where V_p is the peak vibrational velocity and d is the grain diameter. Previous disparate results for the scaling α in power law (1), relating T and V_p, are clarified and explained once we correctly incorporate the role of gravitational potential energy. In particular, we showed that $\alpha = 2$ for all systems in the absence of gravity or when W is high enough. In intermediate regimes, α depends significantly on the range of W employed to fit (1). In these regimes, the change in the barycentric height cannot be employed as a substitute to T.

Our computations suggest that, except at high values of W, modeling temperature T through a power law of form (1) will not be straightforward. In fact, we saw that a sum of two algebraic power laws is better able to capture the response of T with W, cf. (6). However, whenever a power law of kind (1) is sought, given that T depends on W, it is necessary that granular temperature be investigated over a universal range of W. One example of such a universal range is $W_f \leqslant W \leqslant W_2$, where grains are fully fluidized for $W \geqslant W_f$, and gravity may be safely ignored for $W \geqslant W_2$. We also observed that the effect of other system parameters such as e_p, μ_p, N, and A/d did not affect the granular temperature as significantly as W. Thus, the scaling α was regulated most by W, which, in turn, estimates the relative importance of gravitational potential energy vis-a-vis vibrational kinetic energy supplied by the base.

Finally, we investigated the spatial variation of the local temperature $\hat{T}_z$ and the volume fraction $\hat{\phi}$. We saw that both temperature and density peak away from the base at high W. Further, a quadratic scaling of $\hat{T}_z$ is only observed at high W, just as for the volume-averaged temperature T_z. Surprisingly, T_z achieves a quadratic scaling with V_p earlier than does $\hat{T}_z$. These aspects do not yet have a firm theoretical underpinning. A comprehensive understanding of how temperature varies spatially requires a closer and more detailed analysis.

ACKNOWLEDGMENTS

We acknowledge financial support of DST Grant SR/S3/CE/0053/2010, Government of India. We thank members of the Mechanics and Applied Mathematics Group at IIT Kanpur, especially A. Chatterjee, S. Mahesh, and S. S. Gupta for helpful discussions.

APPENDIX: DISCRETE ELEMENT SIMULATIONS

Newton's second law for the ith grain in a granular assembly may be expressed as

$$m_i \boldsymbol{a}_i = \sum_j \boldsymbol{f}_{ij} + m_i \boldsymbol{b}, \tag{A1}$$

where m_i and $\boldsymbol{a}_i$ are, respectively, the mass and acceleration of grain i, while $\boldsymbol{f}_{ij}$ is the force exerted on the ith grain due to its contact with grain j, and $\boldsymbol{b}$ is the body force per unit mass. Note that $\boldsymbol{f}_{ij}$ is zero when the ith grain has no contacting neighbours. For spherical grains, the angular momentum balance about the center of mass of grain i is given by

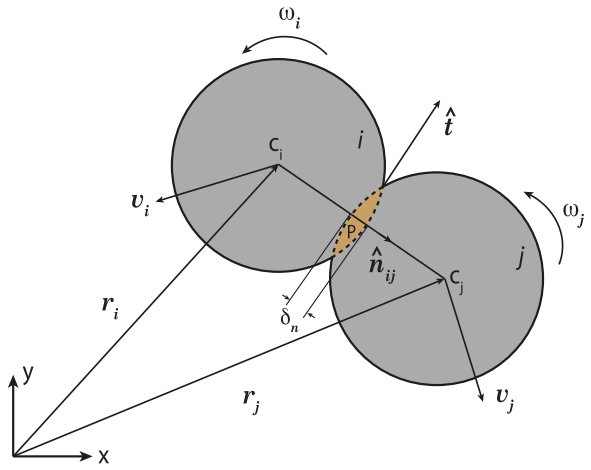

FIG. 17. A two-dimensional schematic representation of contact between two spherical grains with centers C_i and C_j. The normal direction indicated by the unit vector $\hat{\boldsymbol{n}}_{ij}$, while the unit vector $\hat{\boldsymbol{t}}$ indicates the tangential direction.

$$\boldsymbol{I}_i \cdot \boldsymbol{\alpha}_i = \sum_j \boldsymbol{\tau}_{ij}, \tag{A2}$$

where $\boldsymbol{I}_i$ is the mass moment of inertia tensor of grain i about its center of mass, $\boldsymbol{\alpha}_i$ is its angular acceleration, and $\boldsymbol{\tau}_i$ is the total moment exerted on grain i due to its contacting neighbours, which are indexed by j. It is assumed that body force fields do not exert moments.

The interaction between two grains i and j occurs when they touch and subsequently deform, i.e., distance between their centers becomes less than sum of their radii, as shown in Fig. 17. The unit vector $\hat{\boldsymbol{n}}_{ij}$ along the line joining the center of grain i to the center of grain j is defined by

$$\hat{\boldsymbol{n}}_{ij} = \frac{\boldsymbol{r}_{ij}}{|\boldsymbol{r}_{ij}|},$$

where $\boldsymbol{r}_{ij} = \boldsymbol{r}_j - \boldsymbol{r}_i$, with $\boldsymbol{r}_i$ and $\boldsymbol{r}_j$ being the coordinates of the centers of grains i and j with respect to a fixed origin, respectively, so that $|\boldsymbol{r}_{ij}|$ is the distance between their centers. The relative velocity $\boldsymbol{v}_{ij}$ of grain i with respect to grain j at the point of contact P is given by

$$\boldsymbol{v}_{ij} = \boldsymbol{v}_i - \boldsymbol{v}_j + (\boldsymbol{\omega}_i R_i + \boldsymbol{\omega}_j R_j) \times \hat{\boldsymbol{n}}_{ij}, \tag{A3}$$

where "×" denotes the vector cross product, and $\boldsymbol{v}_i$, $\boldsymbol{\omega}_i$, and R_i are the center-of-mass velocity of the ith grain, its angular velocity, and radius, respectively.

The contact force $\boldsymbol{f}_{ij}$ exerted on grain i due to grain j may be decomposed into two components $\boldsymbol{f}^n_{ij}$ and $\boldsymbol{f}^t_{ij}$ that are, hereafter, referred to as the normal and tangential forces of contact, respectively. That is, we write

$$\boldsymbol{f}_{ij} = \boldsymbol{f}^n_{ij} + \boldsymbol{f}^t_{ij}. \tag{A4}$$

We compute normal and tangential forces by employing the linear-spring and dashpot model, where the spring and dashpot are connected in parallel;[31,32] the micro-mechanical model is shown in Fig. 18. The evaluation of spring and damping forces requires estimates of deformation and its rate between colliding grains.

The normal force $\boldsymbol{f}^n_{ij}$ on grain i due to its collision with grain j is

$$\boldsymbol{f}^n_{ij} = -(c_n \boldsymbol{v}^n_{ij} + k_n \delta_n \hat{\boldsymbol{n}}_{ij}), \tag{A5}$$

where c_n and k_n are the damping constant and the spring stiffness along the normal direction, respectively, while $\boldsymbol{v}^n_{ij}$ is component of the relative velocity $\boldsymbol{v}_{ij}$ along $\hat{\boldsymbol{n}}_{ij}$,

$$\boldsymbol{v}^n_{ij} = (\boldsymbol{v}_{ij} \cdot \hat{\boldsymbol{n}}_{ij}) \hat{\boldsymbol{n}}_{ij},$$

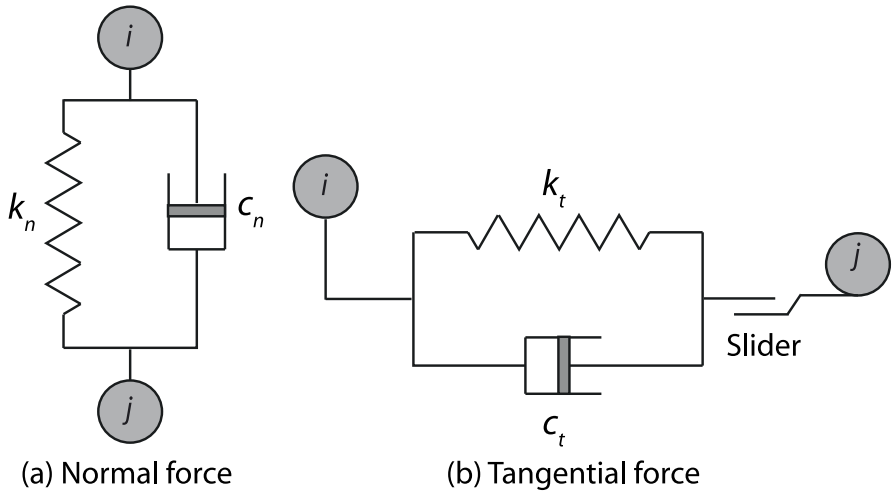

FIG. 18. The general micro-mechanical model for normal and tangential contact forces between two spheres i and j. The various parameters in the figure are defined in the text.

and the overlap δ_n between two contacting grains in the normal direction is estimated by subtracting the distance between their centers from sum of their radii,

$$\delta_n = R_i + R_j - |\boldsymbol{r}_{ij}|, \tag{A6}$$

in terms of the radii R_i and R_j of grains i and j, respectively.

The tangential component of the total force is given by

$$\boldsymbol{f}^t_{ij} = -c_t\, \boldsymbol{v}^t_{ij}, \tag{A7}$$

where c_t, k_t, and $\boldsymbol{v}^t_{ij} = \boldsymbol{v}_{ij} - \boldsymbol{v}^n_{ij}$ are, respectively, the damping constant, the spring stiffness, and the relative velocity along the tangent,

$$\hat{\boldsymbol{t}} = \frac{\boldsymbol{v}^t_{ij}}{|\boldsymbol{v}^t_{ij}|}.$$

As mentioned earlier, we do not include a tangential spring in current simulations, i.e., $k_t = 0$. The Coulomb friction criterion is employed to incorporate friction between two colliding grains, and slipping occurs when the tangential force exceeds $\mu\,|\boldsymbol{f}^n_{ij}|$, so that

$$\boldsymbol{f}^t_{ij} = -\min(c_t \boldsymbol{v}^t_{ij},\, \mu_p\, |\boldsymbol{f}^n_{ij}|\, \hat{\boldsymbol{t}}), \tag{A8}$$

where μ_p is the coefficient of dry friction between surfaces of the colliding grains.

In the linear-spring dashpot model, an analytical relationship between the damping constant c_n and the coefficient of normal restitution e_n may be derived[24,33] by solving the equations of motion of two colliding grains,

$$c_n = \frac{2\,\ln e_n\,\sqrt{k_n\, m}}{\sqrt{\pi^2 + (\ln e_n)^2}}, \tag{A9}$$

where $m = m_i\, m_j/(m_i + m_j)$ is the effective or reduced mass of the colliding grains. The above allows us to tune the damper to obtain the desired restitution e_p.

We non-dimensionalize all quantities of interest. The characteristic parameters employed for non-dimensionalization of length and mass units are grain diameter d and mass m, respectively. The characteristic mass m for spherical grains is calculated from the characteristic grain density ρ, i.e., $m = (\pi/6)d^3\rho$. Furthermore, the characteristic time involves particle diameter and the acceleration due to gravity g, i.e., $t = \sqrt{d/g}$. All computational results presented here are made dimensionless by employing these three characteristic parameters.

[1] I. Goldhirsch, "Introduction to granular temperature," Powder Technol. **182**, 130–136 (2008).
[2] C. S. Campbell, "Rapid granular flows," Annu. Rev. Fluid Mech. **22**, 57–92 (1990).
[3] J. H. Jeans, *An Introduction to the Kinetic Theory of Gases* (Cambridge University Press, 1982).
[4] J. T. Jenkins and S. B. Savage, "A theory for the rapid flow of identical, smooth, nearly elastic, spherical particles," J. Fluid Mech. **130**, 187–202 (1983).
[5] J. T. Jenkins and M. W. Richman, "Boundary conditions for plane flows of smooth, nearly elastic, circular disks," J. Fluid Mech. **171**, 53–69 (1986).
[6] S. Warr, J. M. Huntley, and T. H. Jacques, "Fluidization of a two-dimensional granular system: Experimental study and scaling behavior," Phys. Rev. E **52**(5), 5583–5595 (1995).
[7] V. Kumaran, "Temperature of a granular material 'fluidized' by external vibrations," Phys. Rev. E **57**(5), 5660–5664 (1998).
[8] J. M. Huntley, "Scaling laws for a two-dimensional vibro-fluidized granular material," Phys. Rev. E **58**(4), 5168–5170 (1998).
[9] S. Luding, H. J. Herrmann, and A. Blumen, "Simulations of two-dimensional arrays of beads under external vibrations: Scaling behavior," Phys. Rev. E **50**(4), 3100–3108 (1994).
[10] K. Feitosa and N. Menon, "Breakdown of energy equipartition in a 2D binary vibrated granular gas," Phys. Rev. Lett. **88**(19), 198301-1–198301-4 (2002).
[11] X. Yang and D. Candela, "Potential energy in a three-dimensional vibrated granular medium measured by NMR imaging," Phys. Rev. Lett. **85**(2), 298–301 (2000).
[12] R. D. Wildman, J. M. Huntley, and D. J. Parker, "Granular temperature profiles in three-dimensional vibrofluidized granular beds," Phys. Rev. E **63**, 061311 (2001).
[13] R. D. Wildman and J. M. Huntley, "Scaling exponents for energy transport and dissipation in binary vibro-fluidized granular beds," Phys. Fluids **15**, 3090–3098 (2003).
[14] C. R. K. Windows-Yule and D. J. Parker, "Center of mass scaling in three-dimensional binary granular systems," Phys. Rev. E **89**, 062206-1–062206-8 (2014).
[15] Y. Lan and A. D. Rosato, "Macroscopic behavior of vibrating beds of smooth inelastic spheres," Phys. Fluids. **7**(8), 1818–1831 (1995).
[16] J. Lee, "Scaling behavior of granular particles in a vibrating box," Physica A **219**, 305–326 (1995).
[17] V. Kumaran, "Kinetic theory for a vibro-fluidized bed," J. Fluid Mech. **364**, 163–185 (1998).
[18] P. Sunthar and V. Kumaran, "Characterization of the stationary states of a dilute vibrofluidized granular bed," Phys. Rev. E **64**, 041303-1–041303-12 (2001).
[19] J. J. Brey, M. J. Ruiz-Montero, and F. Moreno, "Boundary conditions and normal state for a vibrated granular fluid," Phys. Rev. E **62**(4), 5339–5346 (2000).
[20] J. J. Brey, M. J. Ruiz-Montero, and F. Moreno, "Hydrodynamics of an open vibrated granular system," Phys. Rev. E **63**, 061305 (2001).
[21] P. A. Cundall and O. D. L. Strack, "A discrete numerical model for granular assemblies," Geotechnique **29**(1), 47–65 (1979).
[22] G. Metcalfe, S. G. K. Tennakoon, L. Kondic, D. G. Schaeffer, and R. P. Behringer, "Granular friction, coulomb failure, and the fluid–solid transition for horizontally shaken granular materials," Phys. Rev. E **65**, 031302 (2002).
[23] P. M. Reis, R. A. Ingale, and M. D. Shattuck, "Crystallization of a quasi-two-dimensional granular fluid," Phys. Rev. Lett. **96**, 258001 (2006).
[24] B. K. Mishra, "A review of computer simulation of tumbling mills by the discrete element method. I. Contact mechanics," Int. J. Miner. Process. **71**, 73–93 (2003).
[25] C. V. Raman, "The photographic study of impact at minimal velocities," Phys. Rev. **12**(6), 442–447 (1918).
[26] W. Goldsmith, *Impact: The Theory and Physical Behaviour of Colliding Solids* (Edward Arnold Publishers, London, 1960).
[27] C. Thornton and Z. Ning, "A theoretical model for the stick/bounce behaviour of adhesive, elastic-plastic spheres," Powder Technol. **99**, 154–162 (1998).
[28] C. Sorace, M. Louge, M. Crozier, and V. Law, "High apparent adhesion energy in the breakdown of normal restitution for binary impacts of small spheres at low speed," Mech. Res. Commun. **36**, 364–368 (2009).
[29] S. McNamara and E. Falcon, "Simulations of dense granular gases without gravity with impact-velocity-dependent restitution coefficient," Phys. Rev. E **71**, 031302 (2005).
[30] C. R. Wassgren, C. E. Brennen, and M. L. Hunt, "Vertical vibration of a deep bed of granular material in a container," J. Appl. Mech. **63**(3), 712–719 (1996).
[31] Y. Tsuji, T. Tanaka, and T. Ishida, "Lagrangian numerical simulation of plug flow of cohesionless particles in a horizontal pipe," Powder Technol. **71**, 239–250 (1992).
[32] K. Rao and P. Nott, *An Introduction to Granular Flow* (Cambridge University Press, 2008).
[33] T. Pöschel and T. Schwager, *Computational Granular Dynamics: Models and Algorithms* (Springer, 2005).